

Reflecting on Accretion in Neutron Star Low-Mass X-ray Binaries

Renee M. Ludlam¹

¹Department of Physics and Astronomy, Wayne State University, 666 W. Hancock St., Detroit, 48201, MI, U.S.A.

Abstract

Neutron star low-mass X-ray binaries accrete via Roche-lobe overflow from a stellar companion that is $\lesssim 1 M_{\odot}$. The accretion disk in these systems can be externally illuminated by X-rays that are reprocessed by the accreting material into an emergent reflection spectrum comprised of emission lines superimposed onto the reprocessed continuum. Due to proximity to the compact object, strong gravity effects are imparted to the reflection spectrum that can be modeled to infer properties of the NS itself and other aspects of the accreting system. This short review discusses the field of reflection modeling in neutron star low-mass X-ray binary systems with the intention to highlight the work that was awarded the 2023 AAS Newton Lacy Pierce Prize, but also to consolidate key information as a reference for those entering this subfield.

Keywords: accretion, accretion disks — stars: neutron — X-rays: binaries

1 Background

Accretion is a ubiquitous process in the universe occurring on both small scales and large scales (e.g., planet formation to supermassive black holes at the center of galaxies). Generally, this process yields the formation of a flat disk structure as a consequence of angular momentum conservation (i.e., an accretion disk). When an accretion disk is externally illuminated by X-rays, these photons are absorbed and reprocessed by the material in the disk prior to being re-emitted. The emergent photons form a reprocessed continuum spectrum with narrow emission and absorption lines superimposed with characteristics indicative of the physical properties of the material in the disk (e.g., the ionization state, density, and composition, etc). This reprocessed emission emerging

from the accretion disk is referred to in the literature as the ‘reflection spectrum’ (Ross and Fabian, 2005; García and Kallman, 2010).

The most prominent emission line in the reflection spectrum is from the iron (Fe) $K\alpha$ transition. This is due to the fact that Fe is one of the most tightly bound nuclei and able to keep its inner-shell electrons in these highly energetic environments. Other key features of the reflection spectrum are emission lines at lower energy (e.g., oxygen lyman alpha; Madej and Jonker 2011; Madej et al 2014; Ludlam et al 2019b, 2021; Moutard et al 2023, or the Fe L-shell transition; Ludlam et al 2018), the Fe K edge near 7 keV, and the Compton hump near 20 keV due to illuminating photons undergoing Compton scattering when interacting with material in the disk. The intrinsically narrow emission lines are broadened due to Doppler, special, and general relativistic effects.

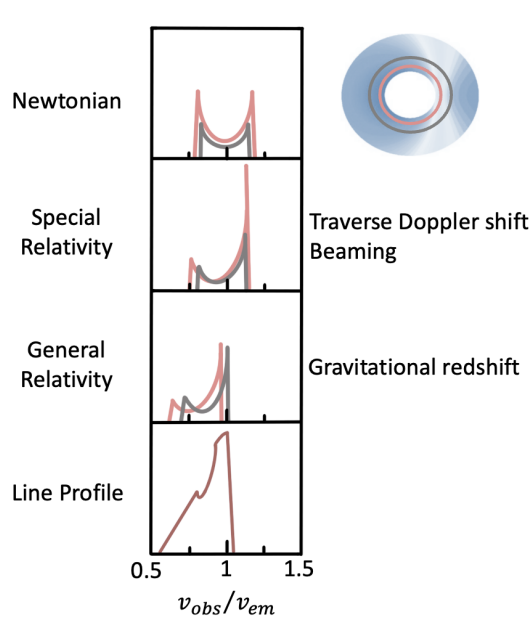


Fig. 1 The impact of different effects on the intrinsically narrow Fe K line profile based on the location within the disk where the emission arises. The annulus in the top right represents the accretion disk with two circle to denote the emission radii shown in the panels (pink close to the compact object and grey further out in the disk). The x-axis shows the broadening effects in terms of the observed line frequency over the emitted frequency (equivalent to energy observed with respect to the energy emitted). Figure adapted from Fabian et al (2000). Classical Newtonian motion leads to Doppler shifts that create a two-horned profile. The rapid rate at which the matter is rotating within the disk leads to Special relativistic effects that creates the asymmetric line profile as photons are beamed into and out of our line of sight. the large gravitational potential well that the disk exists in close to the compact object results in General relativistic effects of gravitational redshift dampening the emission and shifting the photons to lower frequency as they lose energy to escape the strong gravity. The overall line profile is the summation of the emission and effects from different radii.

The strength of these effects depend on the location in which the line emission originates in the accretion disk (Fabian et al, 2000; Dauser, 2010). Figure 1 shows the impact of these effects based on location in the accretion disk.

Relativistically broadened Fe lines indicative of reflection from the inner accretion disk were first observed in Active Galactic Nuclei (AGNs) (Tanaka et al, 1995), which are accreting supermassive black holes (BHs) at the center of galaxies. They were later identified in galactic BH X-ray binaries (XRBs) (Miller et al, 2002) and

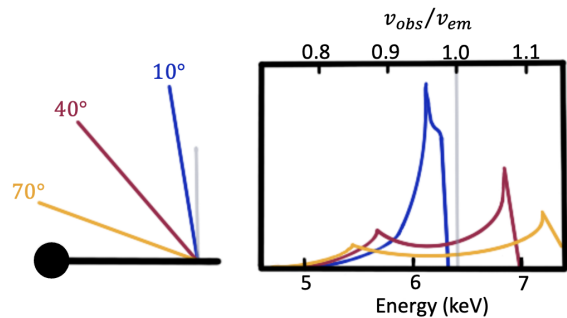


Fig. 2 The effect of inclination on the Fe K line profile adapted from Dauser (2010). Higher inclinations lead to a more extended blue wing of the Fe line profile. Though the example shows the effect of inclination for a maximally spinning BH at different viewing angles, the effect of inclination of the line profile is similar for lower spinning systems, however the gravitational redshift would be less pronounced.

more recently in neutron star (NS) XRBs (Bhatlacharyya and Strohmayer, 2007; Cackett et al, 2008). This suggests a similar accretion geometry in these systems despite the mass difference of the compact accretors vary by orders of magnitude and the presence of a surface in the case of accreting NS. The degree of broadening measured from the Fe line profile in these systems indicated that the line emission indeed arose from the innermost region of the accretion disk.

In the strong gravity regime, general relativity sets the location of the last stable circular orbit of a test particle orbiting an object (Bardeen et al, 1972). For a static (non-rotating) compact object, the location of the innermost stable circular orbit (R_{ISCO}) is 6 gravitational radii ($R_g = GM/c^2$). In the case where a central compact object is rotating prograde (i.e., orbits in the disk are in the same direction as the compact objects angular momentum vector), this distorts the fabric of space-time and supports orbits closer to the BH or NS. Since the gravitational redshift effects on the red-wing of the line profile become stronger closer to the compact object (Fabian et al, 2000), modeling of the Fe line profile enables a measure of the location of the inner disk radius. Additionally, the blue-wing of the line profile is impacted by Doppler effects that strengthen at higher inclinations (Dauser, 2010) (see Figure 2), therefore reflection modeling also enables a measure of the inclination of the system.

Measuring the location of the inner disk in these systems has provided important inferences on the properties of these compact objects. In the case of BHs, this has allowed the measure of the dimensionless spin parameter ($a = cJ/GM^2$), which is one of two physical quantities needed to completely describe an astrophysical BH — the other being mass (see, e.g., [Miller et al 2009](#); [Reynolds 2014, 2021](#) for review). For NSs, the inner disk radius provides an upper limit on the NS radius ([Miller et al, 2013](#); [Ludlam et al, 2017a, 2022](#)) (which has important implications for the equation of state of ultra-dense, cold matter: [Lattimer and Prakash 2001, 2004](#); [Lattimer 2011](#)), magnetic field strength ([Ibragimov and Poutanen, 2009](#); [Cackett et al, 2009](#); [Papitto et al, 2009](#); [Degenaar et al, 2014, 2016](#); [King et al, 2016](#); [Ludlam et al, 2017c](#)), and extent of the boundary layer region extending from the surface of the NS ([Ibragimov and Poutanen, 2009](#); [King et al, 2016](#); [Chiang et al, 2016](#); [Ludlam et al, 2021](#)).

1.1 Controversy for Line Broadening

When broadened Fe line profiles were discovered in BH and NS XRBs, there were alternative origins proposed for the broadening mechanism other than photon reprocessing from the inner disk region. One possible explanation was that the broadening was artificial and arose from pile-up effects in the CCD detectors used on the X-ray missions that were observing these bright galactic sources, e.g., *Chandra* ([Garmire et al, 2003](#)), *Swift* ([Gehrels et al, 2004](#)), *XMM-Newton* ([Jansen et al, 2001](#)), and *Suzaku* ([Mitsuda et al, 2007](#)). Pile-up occurs when two or more low-energy photons interact with the CCD during a single frame readout and register as one higher energy photon. Investigations ([Yamada et al, 2009](#); [Done and Diaz Trigo, 2010](#); [Ng et al, 2010](#)) showed that the line profile did change based upon how the data were extracted (e.g., excising the brightest regions of the detector), but this effect was ultimately demonstrated to artificially narrow the line emission ([Miller et al, 2010](#)), leading to underestimates of the inner disk radius location. Additionally, broadened Fe lines were detected with *RXTE/PCA* which has no pile-up effects ([García et al, 2014b](#)), thus lending to the credibility of the broadening being astrophysical. Further advances in X-ray detectors, such as the CZT detectors on

NuSTAR ([Harrison et al, 2013](#)) and the silicon-drift detectors on *NICER* ([Gendreau et al, 2012](#)), eliminate pile-up effects (except at extremely high count rates of 10^5 counts s^{-1} in the case of *NuSTAR*) and provide an unhindered view of line broadening effects. Figure 3 shows a gallery of Fe line profiles observed with *NuSTAR* that are unbiased by pile-up effects, as well as a more recent example from *NICER*.

Another proposed explanation for the broadening of the observed Fe line profiles was scattering interactions with winds as the photons left the system ([Laurent and Titarchuk, 2007](#); [Titarchuk et al, 2009](#); [Díaz Trigo et al, 2012](#)). However, these broadened lines were observed in hard spectral states for BH XRBs when winds were not present ([Miller et al, 2012](#)) and no significant correlation was found between line width and column density of wind in different NS systems ([Cackett and Miller, 2013](#)). This supports a dynamical origin for the line broadening in these systems. Today the effects of the inner disk as the source of broadening in the reflection spectrum is a generally agreed upon idea. However, there remains controversy over the proper spectral modeling description of the emission from different states, which is discussed further in the next section.

1.2 Emission from NS LMXBs

A NS low-mass X-ray binary (LMXB) accretes via Roche-lobe overflow from a stellar companion that is $\lesssim 1 M_{\odot}$ (for a recent comprehensive reference on LMXBs, see [Bahramian and Degenaar 2023](#)). The accretion in these systems can be persistent or go through transient periods of accretion activity and quiescence (where little to no accretion occurs). The persistently accreting systems fall into one of two categories: ‘Z’ or ‘atoll’. These names refer to characteristic shapes traced out when looking at the ratio of different energy bands (color-color diagrams) or ratio of the hard X-ray band to the soft X-ray band versus of the overall intensity (hardness-intensity diagram; [Hasinger and van der Klis 1989](#)). The division between the two classes is thought to be driven in part by the overall level of mass accretion rate in the system since atolls accrete at a lower Eddington ratio than Z sources (~ 0.01 – $0.5 L_{\text{Edd}}$ for atolls versus ~ 0.5 – $1.0 L_{\text{Edd}}$ for Z sources: [van der Klis 2005](#)). Evidence supporting this comes from transiently

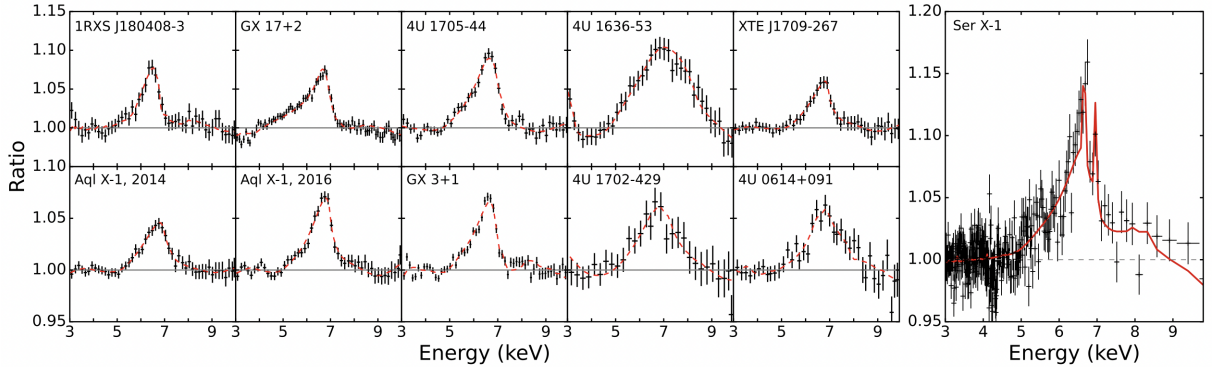


Fig. 3 (*Left:*) Gallery of Fe line profiles observed with *NuSTAR* in accreting NS LMXBs. The ratio is the data to a simple continuum model. The red dashed line indicates the Fe line predicted from reflection modeling with the RELXILL suite of models. The specifics for each source are given in their respective publication: 1RXS J180408-3 (Ludlam et al, 2016); GX 17+2, 4U 1705-44, and 4U 1636-53 (Ludlam et al, 2017a); XTE J1709-267 (Ludlam et al, 2017b); Aquila X-1 (Aql X-1) (Ludlam et al, 2017c); GX 3+1, 4U 1702-429, and 4U 0614+091 (Ludlam et al, 2019a). (*Right:*) The Fe line profile of Serpens X-1 (Ser X-1) observed with *NICER* and reported in Ludlam et al (2018). The solid red line indicates the line profile predicted from fitting RELXILLNS to the data. The energy resolution of *NICER* (~ 137 eV at 6 keV) provides additional detail regarding the structure of the Fe line profile in this system. The double-peaked broad line is a result of high disk density ($\sim 10^{19}$ cm $^{-3}$) allowing both the Fe XXV and Fe XXVI K_{α} lines to fluoresce at a similar intensity. The low inclination of the system prevents the two lines from blurring together.

accreting systems that switched between atoll-like behavior to Z-like behavior over the course of its outburst as the mass accretion rate changes (e.g., XTE J1701–462: Homan et al 2010, and more recently 1A 1744–361: Ng et al 2023).

As mentioned previously, the presence of broadened Fe lines indicates a similar accretion geometry between BH and NS XRBs. BH XRBs exhibit a number of spectral states with varying accretion geometries as the overall accretion rate changes, which requires different models and parameter values in each state (see Done et al 2007 for a review). Unsurprisingly, NS LMXBs also exhibit a number of spectral states that vary considerably and require different models and spectral parameters to describe the continuum emission (Barret, 2001) with the additional complexity of the presence of the NS surface that is not present in BH systems. Various models are used to describe the relative contribution from the presence of the corona (Sunyaev et al, 1991), accretion disk, surface of the NS and/or boundary layer region (where the material from the accretion disk meets the surface of the NS: Popham and Sunyaev 2001; Inogamov and Sunyaev 1999) in each state.

Transient NS LMXBs can exhibit very hard spectral states at the start of an outburst (Ludlam et al, 2016; Parikh et al, 2017; Fiocchi et al,

2019) where the spectrum is dominated by Comptonization from the corona region with little to no emission detected from the accretion disk or NS surface. This extreme hard state can be modeled with an absorbed power-law component with a photon index $\Gamma \sim 1$ (Ludlam et al, 2016; Parikh et al, 2017) or two thermal Comptonization components assuming there is a two temperature coronal plasma with distinct populations of seed photons (Fiocchi et al, 2019). In the hard state, the spectrum is dominated by a hard Comptonization component from the corona with a steeper photon index of $\Gamma = 1.5\text{--}2.0$ and the addition of a soft thermal component with a temperature of $kT \lesssim 1$ keV (Barret et al, 2000; Church and Balucińska-Church, 2001), which arises either from a single temperature blackbody component from the NS surface and/or boundary layer region, or from a multi-color disk blackbody emitted by the accretion disk.

In the soft state, the spectrum becomes thermally dominated by the accretion disk emission or from emission near the NS with weakly Comptonized radiation. Model choices differ to describe the overall continuum in the soft state. Historically, this led to two classical descriptions in the literature: the “Eastern” and “Western” models. The Eastern model, after Mitsuda et al (1989),

uses a multi-color disk blackbody for the accretion disk in combination with a Comptonized single-temperature blackbody component arising from Comptonized photons from a boundary layer region. The Western model, after [White et al \(1988\)](#), uses a single-temperature blackbody to model emission from the NS or boundary layer with a Comptonized accretion disk component.

A hybrid model was devised by [Lin et al \(2007\)](#) to build a coherent picture of the spectral evolution between the hard and soft state spectra using *RXTE* observations of two transient atoll systems. In this model, the soft state assumes two thermal components (i.e., a single-temperature blackbody and an accretion disk blackbody) and weak Comptonization that is accounted for by a power-law component. The thermal components followed the expected $L_x \propto T^4$ relation as the mass accretion rate ($\dot{m} \propto L_x$) changed between states ([Lin et al, 2007](#)). Although this hybrid double thermal model has been used in many NS LMXBs studies (e.g., [Cackett et al 2008, 2009](#); [Lin et al 2010](#); [Miller et al 2013](#)), the various soft state model prescriptions are still utilized. A recent study used a model akin to the “Eastern” model (i.e., thermal Comptonization from a blackbody and a multi-color accretion disk blackbody) for the X-ray spectra of the atoll 4U 1820-30 and found good agreement between the changes in the Comptonized blackbody with the observed jet variability in this system ([Marino et al, 2023](#)). Hence, spectral models that can describe data equally well in the X-ray band benefit from the additionally information provided by multi-wavelength data. In the absence of multi-wavelength data to support a choice of continuum model, it is difficult to ascertain which prescription of the spectra is appropriate and multiple model descriptions need to be explored.

The exact geometry of the corona also remains a subject of mystery (see [Degenaar et al 2018](#) for some possible geometries). However, the recent operation of the *Imaging X-ray Polarization Explorer (IXPE)* ([Weisskopf et al 2022](#)) has enabled X-ray polarization measurements for a handful of accreting NSs which are beginning to shed light on the coronal orientation and presence of boundary layer regions in these systems (e.g., [Jayasurya et al 2023](#); [Ursini et al 2023](#); [Cocchi et al 2023](#); [Farinelli et al 2023](#)). Similar to multi-wavelength studies, X-ray polarization measurements aid in building up our understanding of the accretion

geometry when coupled with X-ray energy spectral studies. Although the choice of continuum impacts the interpretation of the accretion geometry and relative contribution of each component in the various spectral states, reflection studies have shown that the choice of continuum does not impact the results significantly, as long as the reprocessed emission is treated in a consistent manner with the assumed illumination component ([Coughenour et al, 2018](#); [Ludlam et al, 2020](#)).

2 Reflection Modeling

Modeling the reflection spectrum to infer properties of the accreting system originally used single line emission models ([Fabian et al, 1989](#); [Laor, 1991](#)). However, we know that the reflection spectrum is a modified continuum with multiple atomic emission lines hence a full reflection model framework should be used to properly describe all the reprocessed emission. Eventually more sophisticated model grids were developed that encompassed the reprocessed continuum from irradiation of a constant density medium with varying illumination continua ([Magdziarz and Zdziarski, 1995](#); [Ross et al, 1999](#); [García and Kallman, 2010](#); [García et al, 2011, 2013, 2022](#)). Additionally, ad-hoc convolution reflection models were created that piece together expected shapes in different energy bands, such as RFXCONV ([Done and Gierliński, 2006](#); [Kolehmainen et al, 2011](#)), which generates an angle-dependent reflection spectrum from a Comptonized input spectrum by combining the reflection emission from an ionized disk interpolated from REFLIONX ([Ross and Fabian, 2005](#)) below 14 keV (using the average 2–10 keV power-law index) with Compton reflected emission from PEXRIV ([Magdziarz and Zdziarski, 1995](#)) above 14 keV (using the average 12–14 keV power-law index).

These reprocessed emission models needed to be blurred with convolution kernels to account for Doppler, special, and general relativistic effects, such as ‘rdblur’ (modified from DISKLINE for non-spinning BHs: [Fabian et al 1989](#)), ‘kdblur’ (modified from LAOR for maximally rotating BHs: [Laor 1991](#)), ‘kerrconv’ ([Brenneman and Reynolds, 2006](#)), and ‘relconv’ ([Dauser, 2010](#)) (the latter two have the spin of the compact object is a free parameter). As the available models for the reflection spectrum and convolution kernel

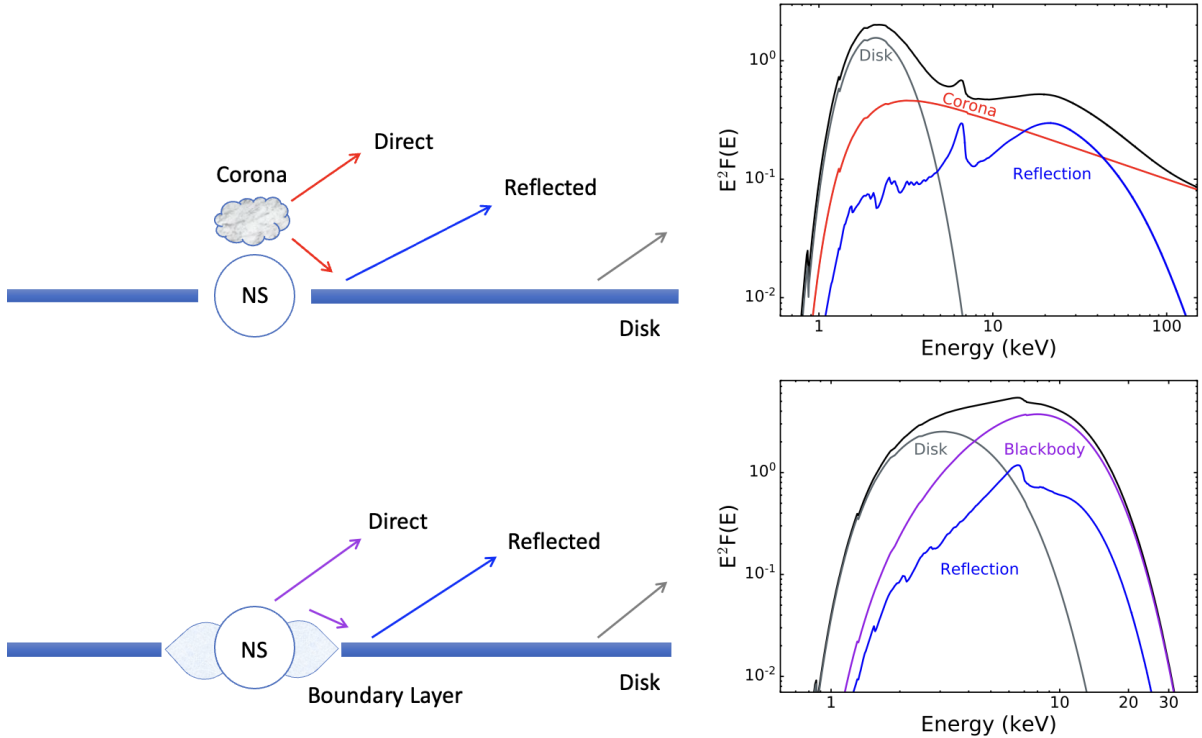


Fig. 4 Simplistic representation of emission of a NS accreting from a geometrically thin, optically thick accretion disk in a hard coronally-dominated spectral state (top) and soft thermally-dominated spectral state (bottom). The resulting unfolded model versus energy from these states are shown in the panels on the right using arbitrary values. The thermally dominated state has a significantly softer spectrum than a coronally-dominated state. This demonstrates how the external illumination component (either a power-law or blackbody irradiating the disk) shapes the reprocessed emission.

became sophisticated, the development of a self-consistent reflection model that traces the path of each photon from the system to construct the emergent spectrum was created in 2014 known as RELXILL (Dauser et al, 2014; García et al, 2014a). The model convolves XILLVER (García and Kallman, 2010; García et al, 2011, 2013) reflection model tables with the blurring kernel of ‘relconv’ (Dauser, 2010; Dauser et al, 2013). Within RELXILL, the model chooses the appropriate reflection spectrum at each disk radius for each emission angle calculated in a curved space-time, which consequently accurately captures the detailed dependence of the emitted reflection spectrum with the viewing angle.

2.1 Parameters of RELXILL with respect to NS LMXBs

A comprehensive explanation of parameter definitions in the RELXILL suite of models is given on the

developers website¹. We briefly cover these parameters here as similar parameters are used in other existing reflection models and how they relate to reflection studies in accreting NS systems. The reflection grids are generated based on an illuminating continuum input (i.e., the ‘primary source’) and thus result in different flavors of the model. For example, RELXILL has a cut-off power-law with photon index Γ and cut-off energy E_{cut} as the illuminating photon distribution, whereas RELXILLNS (García et al, 2022) was designed assuming thermal illumination from the NS or boundary layer region with a temperature of kT_{bb} . There is a flavor of RELXILL with a Comptonization illuminating continuum known as RELXILLCP, however this assumes the seed photons arise from the accretion disk with a fixed temperature of 0.01 keV that is appropriate for BHs but too low for NS

¹https://www.sternwarte.uni-erlangen.de/~dauser/research/relxill/relxill_docu_v1.0.pdf

systems (Ludlam et al, 2019a). Hence, RFXCONV is typically used when modeling reflection from Comptonization in NS systems. Figure 4 provides a simplistic, toy-model representation of the accretion geometry in a hard and soft spectral state to demonstrate the difference in the overall resulting spectral shape given illumination by a power-law versus a blackbody component. García et al (2022) provides a more in-depth comparison of the input models and resulting reflection spectral shape.

The emissivity profile, q , in reflection modeling characterizes the illumination pattern of the accretion disk by the primary source and is a radially dependent prescription of r^{-q} . Whether the emissivity index is a positive or negative value depends on how the model was defined. Given that these models were designed for the extreme gravity near a BH, the models allow for two emissivity index profiles for illumination of the inner disk region where strong gravitational light bending effects cause steep profiles (q_1) and outer region of the accretion disk where effects are less pronounced (q_2) (Wilkins and Fabian, 2012). The break radius (Rbr) sets the location in the disk where the emissivity index changes from q_1 to q_2 in units of R_g . However, in NS systems, the gravitational effects are less extreme and a single emissivity profile is used (i.e., $q_1 = q_2$, hence Rbr is obsolete) with an expected value $q < 5$ (Cackett et al, 2010). Indeed, theoretical emissivity profile calculations through ray-tracing simulations from a hotspot on the surface of the NS or boundary layer region support a single emissivity index close to the expected value for flat, Euclidean geometry (Wilkins, 2018). Some studies elect to fix the emissivity index at $q = 3$ for the flat, Euclidean geometry (e.g., Sleator et al 2016; Degenaar et al 2016; Ludlam et al 2017b,c; Mondal et al 2018, 2020; Coughenour et al 2018), however, for the majority of studies where the emissivity index is left as a free parameter a value between $1.5 < q < 4$ is typically found (e.g., Miller et al 2013; Matranga et al 2017; Ludlam et al 2016, 2017a, 2018, 2019a, 2020, 2021, 2023; Saavedra et al 2023; Moutard et al 2023).

The extent of the accretion disk is set by the inner disk radius (R_{in} , in units of R_{ISCO} or R_g depending on the model) and outer disk radius (R_{out} , in units of R_g). R_{in} is typically left free to vary, whereas R_{out} is fixed at or near the maximum value allowed by the model. The inclination

(i) of the system with respect to our line of sight is given in degrees. The cosmological redshift to the source is defined by z . However, for most of the analyses discussed here this parameter is fixed at 0 since the sources of interest are galactic. The normalization of the RELXILL suite of models is discussed in detail in (Dauser et al, 2016).

As previously mentioned in §1, the dimensionless spin parameter (a) sets the location of the innermost stable circular orbit of the accretion disk (R_{ISCO}). The majority of galactic NSs in LMXBs have spin $a \lesssim 0.3$ (Galloway et al, 2008; Miller et al, 2011). The difference in the location of R_{ISCO} between $a = 0$ and $a = 0.3$ is $\sim 1 R_g$ in the Kerr metric (Bardeen et al, 1972). Deviations from the Kerr metric may occur as rotation of the NS increases and induces a quadrupole moment as the NS becomes oblate, however, the Kerr metric remains a good approximation. The exact deviation from the Kerr metric depends upon the equation of state (EoS) which remains elusive, but at $a = 0.3$ the deviations from an induced quadrupole moment is at most 10% (Sibgatullin and Sunyaev, 1998). This becomes a larger deviation ($\sim 25\%$, see Figure 1 in Sibgatullin and Sunyaev 1998) closer to rotation limit of the NS ($a \sim 0.7$), where the centrifugal force overcomes the self-gravity of the NS. There is an approximation for spin relating to measured spin periods of NSs in units of milliseconds ($a = 0.47/P_{\text{ms}}$: Braje et al 2000), but it is important to note that this assumes a softish EOS of the ‘‘FPS’’ model (Cook et al, 1994) and canonical values for NS mass and radius ($M_{\text{NS}} = 1.4 M_{\odot}$, $R_{\text{NS}} = 10 \text{ km}$). Given limitations with data quality and the degenerate nature between a and R_{ISCO} , the spin is fixed at a value in reflection modeling while the inner disk radius (R_{in}) is free to vary. Future mission concepts may provide the necessary data quality to determine both parameters (Ludlam et al, 2023).

These models allow for variation in the abundance of iron, A_{Fe} , with respect to solar abundance. The value of A_{Fe} impacts the shape of the reprocessed continuum as well as the relative strength of the emission from different atomic species (e.g., see Figure 4 of García et al 2022). A number of galactic accreting XRBs were inferred to have super-solar Fe abundance ($A_{\text{Fe}} \gtrsim 5$; e.g., Tomsick et al 2018; Ludlam et al 2018, 2019a, 2017a; Connors et al 2021; Liu et al 2023), but this could be remedied by models that allowed

for higher disk density values than the standard value of 10^{15} cm^{-3} (García et al, 2018; Tomsick et al, 2018). The disk density of 10^{15} cm^{-3} is a value appropriate for AGN accretion disks that spawned the field of reflection modeling, however, the accretion disks around stellar mass BHs and NSs are expected to have densities $\geq 10^{20} \text{ cm}^{-3}$ (Shakura and Sunyaev, 1973; Frank et al, 2002). García et al (2016, 2018) provide more details about the effect of disk density on the reprocessed emission spectrum. Some flavors of RELXILL have a variable disk density parameter, $\log(n_e/\text{cm}^{-3})$, with an upper limit of 19 or 20 depending on the model. The development of RELXILL models with densities $\log(n_e/\text{cm}^{-3}) > 20$ is an active area of development (Ding et al. 2023, *submitted*), though there are some REFLIONX grids currently available² that can be blurred with relativistic blurring kernels (Tomsick et al, 2018; Connors et al, 2021; Liu et al, 2023).

The ionization state of the accreting material can be constrained from modeling of the reflection spectrum. The ionization parameter, $\log(\xi/\text{erg cm s}^{-1})$, is defined as $\xi = 4\pi F_x/n_e$ based on the definition from Tarter et al (1969) (F_x is the illuminating flux and n_e is the disk density), can vary to describe a nearly neutral (0) to highly ionized (4.7) medium. The ionization state of the medium changes the overall spectral shape of the reflection spectrum which also varies as a function of disk density (see Figure 3 of García et al 2022 for thermal illumination of disks of varying density). The ionization parameters of NS LMXBs are typically moderate depending on the spectral state ($\log(\xi) = 2.3\text{-}4.0$: Cackett et al 2010; Ludlam et al 2017a, 2019a)

Another explicit parameter of the reflection models is the reflection fraction. Note that the model creators refer to this parameter as R_f or R_{frac} , but I will use f_{refl} to avoid confusion with parameters that use R to refer to radius. Due to strong gravitational light-bending effects close to these accreting compact objects, f_{refl} is defined from the reference frame of the primary source as the ratio of emitted photons that will interact with the disk versus those that will be directly emitted to infinity (Dauser et al, 2016). Consequently, it is possible for this to have a value greater than unity if the location of the illumination source is closer

to the accretion disk and deeper in the gravitational well where light-bending effects strengthen, since the majority of emitted photons would interact with the disk with relatively fewer emitted towards infinity.

One special flavor of RELXILL that has yet to be publicly released³ is that used for the subclass of LMXBs known as ultra-compact X-ray binaries (UCXBs). These systems have orbital periods of < 90 minutes that indicates that the donor star cannot be a main-sequence star but rather a degenerate stellar companion like a white dwarf. Since the donor has a significantly different chemical composition that is nearly devoid of hydrogen and helium while overabundant in carbon and oxygen (Nelemans et al, 2004), special models are necessary. XILLVERCO was created to be able to model these unique reflection spectra that have low energy relativistically broadened O lines with weak Fe K lines (Madej and Jonker, 2011; Madej et al, 2014; Ludlam et al, 2019b, 2021; Moutard et al, 2023). This model has some key differences in comparison to others, such as a variable abundance of carbon and oxygen, A_{CO} , rather than A_{Fe} . The primary source input is a cut-off power law but the model also takes into account the local thermal radiation from below by the accretion disk itself, the ratio these components is defined by the ‘Frac’ parameter. The rest of the parameters resemble those of the RELXILL suite described above. More detailed information about the XILLVERCO model can be found in Madej et al (2014); Ludlam et al (2021).

2.2 Results of reflection modeling

Reflection modeling has provided us with an additional method to infer the location of the inner disk radius based upon measuring the degree of relativistic effects impacting emission line profiles. As mentioned in § 1, measuring the location of the inner disk allows us to infer key properties of the NSs in these systems. There are a number of methods to determine the radii of NSs in order to determine the EOS of ultra-dense, cold matter (see Özel and Freire 2016 for a review of different methodologies). Reflection spectroscopy offers an independent and complementary approach to

²<https://www.michaelparker.space/reflionx-models>

³The reflection model for UCXBs is available upon request to the author or J. A. García.

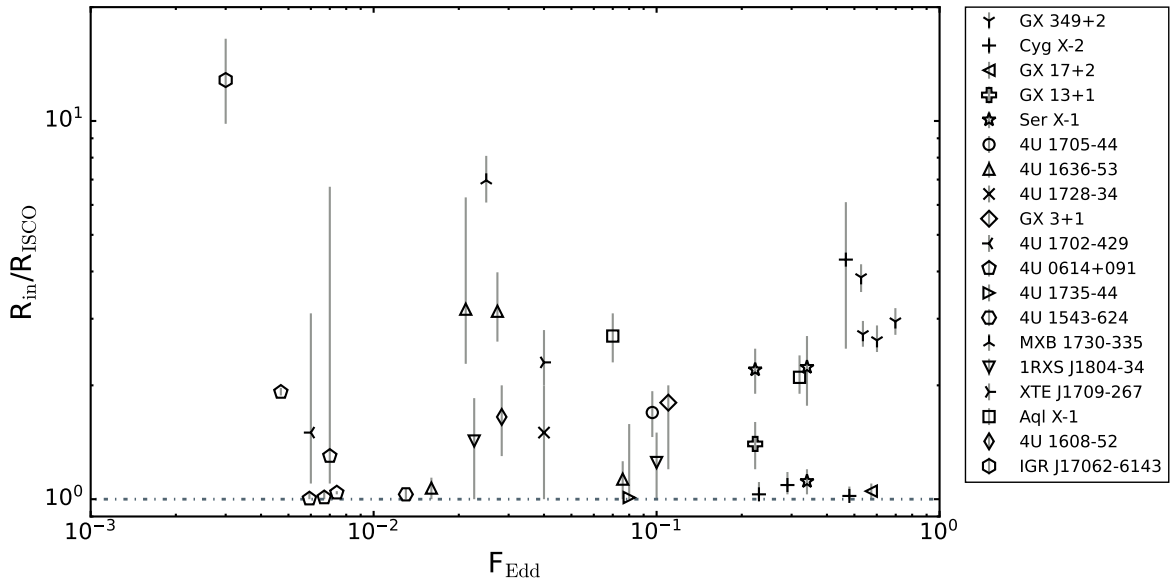


Fig. 5 Measured inner disk radius (R_{in}) in terms of R_{ISCO} from reflection modeling versus the Eddington fraction ($F_{\text{Edd}} = L_{0.5-50\text{keV}}/L_{\text{Edd}}$), which is a proxy for mass accretion rate (\dot{m}), for various NS LMXBs. Here, L_{Edd} is the empirical limit of 3.8×10^{38} ergs s^{-1} from [Kuulkers et al \(2003\)](#). The horizontal dot-dashed line indicated $1 R_{\text{ISCO}}$. Figure adapted from [Moutard et al \(2023\)](#). These studies in particular were executed with *NuSTAR* observations and therefore assuredly unbiased by pile-up effects. These sources span several orders of magnitude in mass accretion rate, but no clear trend exists in terms of location of the inner edge of the accretion disk. References for the sources are: GX 349+2 ([Coughenour et al, 2018](#)), Cyg X-2 ([Mondal et al, 2018](#); [Ludlam et al, 2022](#)), GX 13+1 ([Saavedra et al, 2023](#)), Ser X-1 ([Miller et al, 2013](#); [Matranga et al, 2017](#); [Mondal et al, 2020](#)), GX 17+2 & 4U 1705-44 ([Ludlam et al, 2017a](#)), 4U 1636-53 ([Ludlam et al, 2017a](#); [Wang et al, 2017](#)), 4U 1728-34 ([Sleator et al, 2016](#)), GX 3+1 & 4U 1702-429 ([Ludlam et al, 2019a](#)), 4U 0614+091 ([Ludlam et al, 2019a](#); [Moutard et al, 2023](#)), 4U 1735-44 ([Ludlam et al, 2020](#)), 4U 1543-624 ([Ludlam et al, 2021](#)), MXB 1730-624 ([van den Eijnden et al, 2017](#)), 1RXS J1804-34 ([Ludlam et al, 2016](#); [Degenaar et al, 2016](#)), XTE J1709-267 ([Ludlam et al, 2017b](#)), Aql X-1 ([Ludlam et al, 2017b](#)), 4U 1608-52 ([Degenaar et al, 2015](#)), and IGR J17062-6143 ([van den Eijnden et al, 2018](#)).

the current best efforts that are underway (see Figure 5 in [Ludlam et al 2022](#) for a comparison to gravitational wave mergers and pulsar light curve modeling efforts).

An emission radius can also be inferred from the thermal radiation components (multi-color blackbody disk and single-temperature blackbody) in the spectrum. These rely on knowing the distance to the source, which can induce large uncertainties on the radius estimate in the absence of a precise distance measurement (e.g., see Table 5 in [Ludlam et al 2022](#)). Color correction factors are often applied when estimating the thermal emission radius to account for spectral hardening ([Shimura and Takahara, 1995](#); [Kubota et al, 2001](#)). For the disk blackbody component in particular, the inferred inner radius can be overestimated by a factor of > 2 if not accounting for zero-torque inner boundary condition as expected

for thin disk accretion in these systems ([Zimmerman et al, 2005](#)). Additionally, the inferred spherical emission radius of the single-temperature blackbody component can be unphysically small for the emission to be equivalent to the surface of the NS. If however the emission arises from a narrow banded region on the surface of the NS (i.e., the boundary layer/spreading layer; [Inogamov and Sunyaev 1999](#)) with a vertical height that is 5%-10% of the radial extent ([Popham and Sunyaev, 2001](#)), then this can increase the inferred radius to reasonable values ([Ludlam et al, 2021](#)). The extent of the boundary layer region can also be estimated based on the mass accretion rate at the time of the observation by using Equation 25 of [Popham and Sunyaev \(2001\)](#). However, this does not account for the spin of the NS or viscous effects that can impact the radial extent of the boundary layer region. While all of these additional estimates aid in building up a coherent

model of the accretion geometry in these systems, the advantage of reflection modeling to obtain the position of the inner disk radius relies heavily on proper modeling of the effects in the strong gravity regime near the NS.

The existing number of reflection studies in NS LMXBs utilizing data from *NuSTAR* (which are unbiased by pile-up effects) spans several orders of magnitude in mass accretion rate, \dot{m} . As a result, the search for a trend in the location of the inner disk radius as a function of \dot{m} has been investigated. As discussed in the introduction, the presence of reflection in NS LMXBs suggests a similar accretion geometry to BH systems. For BH XRBs, the accretion disk is thought to recede from the compact object at low \dot{m} (see [Done et al 2007](#) for a schematic of the accretion geometry with spectral states/mass accretion rate). Figure 5 shows the measured position of the inner disk radius as a function of Eddington Fraction, which is a proxy of \dot{m} since $L \propto \dot{m}$. There is no clear correlation between position of the inner disk radius as a function of \dot{m} in these systems and this is likely due to the fact that NSs have a surface and an inherent magnetic field.

The strength of the magnetic field differs between sources (with B -fields on the order of $\sim 10^8$ – 10^9 G for LMXBs; [Caballero and Wilms 2012](#)), but can be strong enough to truncate the accretion disk before the ISCO. If the truncation radius inferred from reflection modeling is at the Alfvén radius (where the energy density of the accretion flow equates to the energy density of the NS’s magnetic field), then an upper limit on the strength of the magnetic field can be obtained ([Ibragimov and Poutanen, 2009](#); [Cackett et al, 2009](#)). This technique has been utilized to determine the magnetic field strength of NS LMXBs in the absence of pulsations, which could be shielded from our line of sight by several effects (see [Lamb et al 2009](#) for more details). In particular, a study of the transiently accreting NS LMXB Aquila X-1 (Aql X-1) demonstrated the validity of using reflection modeling to obtain an upper limit on magnetic field strength ([Ludlam et al, 2017c](#)). Figure 6 shows a comparison of estimates from reflection modeling in comparison to the magnetic field strengths from accreting millisecond pulsars (AMXPs) that show pulsations indicative of magnetospheric accretion that were reported in [Mukherjee et al \(2015\)](#). Aql X-1 is also an AMXP, so the agreement between

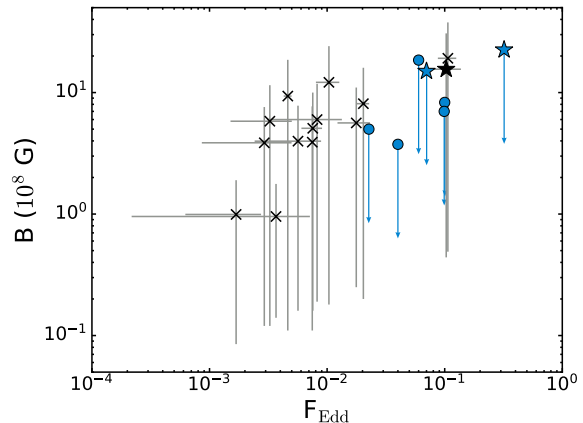


Fig. 6 Magnetic field strength of AMXPs (black crosses and star) in comparison to upper limits inferred from reflection modeling in several NS LMXBs (blue circles and stars). Figure recreated from [Ludlam et al \(2017c\)](#). Of particular interest are the data points for Aquila X-1 (denoted as stars) which is an AMXP with an estimation from pulsations and reflection modeling. The agreement between the two methods for this source verifies that reflection modeling can be used to place limits on NS magnetic field strengths in the absence of discernible pulsations.

the estimation of the B -field from these two methods lends credibility to using reflection modeling for gaining upper limits on magnetic field strength of NSs.

However, the behavior of the inner disk radius with \dot{m} in individual systems needs to be considered to confirm if the magnetic field is responsible for truncation in the absence of detectable pulsations or if the extended boundary layer from the surface of the NS is responsible. If the magnetosphere is strong enough to impede the accretion flow, then the location of the Alfvén radius changes as a function of mass accretion rate ([Ibragimov and Poutanen, 2009](#)). If \dot{m} increases, then the energy density of the accretion flow increases and moves the disk closer to the NS. Conversely, if the boundary layer is responsible for truncation of the inner disk, in accordance with Eq. 25 in [Popham and Sunyaev \(2001\)](#) the radial extent of the boundary layer grows as \dot{m} increases. In this case the inner disk radius would become more truncated. Hence, observing systems with truncated accretion disks over large changes in flux (and thereby \dot{m}) can be used to determine which mechanism is responsible.

At low enough \dot{m} ($F_{\text{Edd}} \lesssim 10^{-2}$), standard thin disk accretion gives way to a radiatively inefficient accretion flow (Narayan and Yi, 1994; Esin et al, 1997). The exact \dot{m} value where this transition occurs is unclear, but monitoring transients as they return to quiescence after outburst provides an opportunity to capture observations in the lowest \dot{m} regime where this is expected to occur. Figure 5 shows that some sources (e.g., 4U 0614+091) with $F_{\text{Edd}} < 0.01$ have a disk that extends down to R_{ISCO} , so it must be possible to still have a standard thin disk down in this regime. Yet, van den Eijnden et al (2020) reported the disappearance of reflection features during the outburst decay of 4U 1608–52 that was observed at $F_{\text{Edd}} \sim 0.002$, which suggested that the accretion disk transitioned to the radiatively inefficient regime. Evidently, the accretion disk flow transitions somewhere between $0.002 \lesssim F_{\text{Edd}} \lesssim 0.006$ and reflection modeling provides a means in narrowing this down further with more dedicated observations as sources decay from outburst.

3 Concluding Remarks

Reflection model studies in NS LMXBs offer an independent method for determining upper limits on radii of NSs and their magnetic field strengths, a probe into accretion when a surface is present (i.e., the presence of a boundary/spreading layer), the prospect to determine when standard thin disk accretion gives way to radiatively inefficient flows at low \dot{m} , and properties of the accreting material itself (e.g., density, composition, ionization state). Additional studies that combine X-ray polarization measurements with reflection studies can aid in furthering our understanding of both the illumination source (i.e., coronal orientation in line with jet or disk) and accretion geometry. These need to be modeled concurrently as the prescription of the energy spectrum does lend to the interpretation of the polarization measurements, hence reflection can provide an independent check in cases where the disk is inferred to be truncated from polarization properties (e.g., Farinelli et al 2023).

Soon we will learn even more about these accreting systems through high energy resolution ($\lesssim 5$ eV) capabilities afforded by the successful launch of *X-Ray Imaging and Spectroscopy Mission (XRISM)*; (Tashiro et al 2018), which is currently in the performance verification phase

and set to begin community driven observations in 2024. The superior energy resolution of the microcalorimeter array onboard will be able to discern between minute differences in available reflection models and provide a more detailed view of the Fe line region to reveal structure due to density effects. In the late 2030s, the Advanced Telescope for High Energy Astrophysics (*Athena*; Nandra et al 2013, recently re-scoped to *NewAthena*), is anticipated to become operational. The microcalorimeter array’s energy resolution will be similar to *XRISM*, but the large collecting area and low background count rate of the Wide Field Imager (WFI; Meidinger 2018) will enable targeting faintly accreting sources in less than half the exposure time needed for currently available facilities in order to understand accretion at low \dot{m} . To aid in how these missions are relevant to reflection modeling, Garca et al (2022) provides simulated *XRISM* spectra showing the difference between two available reflection models and simulated O and Fe line emission profiles based on the anticipated capabilities with *Athena*. Reflection modeling is an advantageous technique to infer properties of accreting NSs and will undoubtedly enhance our understanding of these systems into the future.

References

- Bahramian A, Degenaar N (2023) Low-Mass X-ray Binaries. In: Handbook of X-ray and Gamma-ray Astrophysics. Edited by Cosimo Bambi and Andrea Santangelo. p 120, https://doi.org/10.1007/978-981-16-4544-0_94-1
- Bardeen JM, Press WH, Teukolsky SA (1972) Rotating Black Holes: Locally Nonrotating Frames, Energy Extraction, and Scalar Synchrotron Radiation. *ApJ*178:347–370. <https://doi.org/10.1086/151796>
- Barret D (2001) The broad band x-ray/hard x-ray spectra of accreting neutron stars. *Adv Space Res* 28(2-3):307–321. [https://doi.org/10.1016/S0273-1177\(01\)00414-8](https://doi.org/10.1016/S0273-1177(01)00414-8), [arXiv:astro-ph/0101295](https://arxiv.org/abs/astro-ph/0101295) [astro-ph]
- Barret D, Olive JF, Boirin L, et al (2000) Hard X-Ray Emission from Low-Mass X-Ray Binaries. *ApJ*533(1):329–351. <https://doi.org/10.1086/317000>

- 1086/308651, [arXiv:astro-ph/9911042](https://arxiv.org/abs/astro-ph/9911042) [astro-ph]
- Bhattacharyya S, Strohmayer TE (2007) Evidence of a Broad Relativistic Iron Line from the Neutron Star Low-Mass X-Ray Binary Serpens X-1. *ApJL*664(2):L103–L106. <https://doi.org/10.1086/520844>, [arXiv:0708.3648](https://arxiv.org/abs/astro-ph/0708.3648) [astro-ph]
- Braje TM, Romani RW, Rauch KP (2000) Light Curves of Rapidly Rotating Neutron Stars. *ApJ*531(1):447–452. <https://doi.org/10.1086/308448>, [arXiv:astro-ph/0004411](https://arxiv.org/abs/astro-ph/0004411) [astro-ph]
- Brenneman LW, Reynolds CS (2006) Constraining Black Hole Spin via X-Ray Spectroscopy. *ApJ*652(2):1028–1043. <https://doi.org/10.1086/508146>, [arXiv:astro-ph/0608502](https://arxiv.org/abs/astro-ph/0608502) [astro-ph]
- Caballero I, Wilms J (2012) X-ray pulsars: a review. *Mem. Soc. Astron. Italiana*83:230. <https://doi.org/10.48550/arXiv.1206.3124>, [arXiv:1206.3124](https://arxiv.org/abs/1206.3124) [astro-ph.HE]
- Cackett EM, Miller JM (2013) Broad Iron Lines in Neutrons Stars: Dynamical Broadening or Wind Scattering? *ApJ*777(1):47. <https://doi.org/10.1088/0004-637X/777/1/47>, [arXiv:1308.4023](https://arxiv.org/abs/1308.4023) [astro-ph.HE]
- Cackett EM, Miller JM, Bhattacharyya S, et al (2008) Relativistic Iron Emission Lines in Neutron Star Low-Mass X-Ray Binaries as Probes of Neutron Star Radii. *ApJ*674(1):415–420. <https://doi.org/10.1086/524936>, [arXiv:0708.3615](https://arxiv.org/abs/0708.3615) [astro-ph]
- Cackett EM, Altamirano D, Patruno A, et al (2009) Broad Relativistic Iron Emission Line Observed in SAX J1808.4–3658. *ApJL*694(1):L21–L25. <https://doi.org/10.1088/0004-637X/694/1/L21>, [arXiv:0901.3142](https://arxiv.org/abs/0901.3142) [astro-ph.HE]
- Cackett EM, Miller JM, Ballantyne DR, et al (2010) Relativistic Lines and Reflection from the Inner Accretion Disks Around Neutron Stars. *ApJ*720(1):205–225. <https://doi.org/10.1088/0004-637X/720/1/205>, [arXiv:0908.1098](https://arxiv.org/abs/0908.1098) [astro-ph.HE]
- Chiang CY, Morgan RA, Cackett EM, et al (2016) On the Evolution of the Inner Disk Radius with Flux in the Neutron Star Low-mass X-Ray Binary Serpens X-1. *ApJ*831(1):45. <https://doi.org/10.3847/0004-637X/831/1/45>
- Church MJ, Balucińska-Church M (2001) Results of a LMXB survey: Variation in the height of the neutron star black-body emission region. *A&A*369:915–924. <https://doi.org/10.1051/0004-6361:20010150>, [arXiv:astro-ph/0102019](https://arxiv.org/abs/astro-ph/0102019) [astro-ph]
- Cocchi M, Gnarini A, Fabiani S, et al (2023) Discovery of strongly variable X-ray polarization in the neutron star low-mass X-ray binary transient XTE J1701–462. *A&A*674:L10. <https://doi.org/10.1051/0004-6361/202346275>, [arXiv:2306.10965](https://arxiv.org/abs/2306.10965) [astro-ph.HE]
- Connors RMT, García JA, Tomsick J, et al (2021) Reflection Modeling of the Black Hole Binary 4U 1630–47: The Disk Density and Returning Radiation. *ApJ*909(2):146. <https://doi.org/10.3847/1538-4357/abdd2c>, [arXiv:2101.06343](https://arxiv.org/abs/2101.06343) [astro-ph.HE]
- Cook GB, Shapiro SL, Teukolsky SA (1994) Rapidly Rotating Neutron Stars in General Relativity: Realistic Equations of State. *ApJ*424:823. <https://doi.org/10.1086/173934>
- Coughenour BM, Cackett EM, Miller JM, et al (2018) A NuSTAR Observation of the Low-mass X-Ray Binary GX 349+2 throughout the Z-track. *ApJ*867(1):64. <https://doi.org/10.3847/1538-4357/aae098>, [arXiv:1708.01652](https://arxiv.org/abs/1708.01652) [astro-ph.HE]
- Dauser T (2010) Theoretical Modeling of Broad Emission Lines. Master’s thesis, Friedrich Alexander University of Erlangen-Nuremberg, Germany
- Dauser T, García J, Wilms J, et al (2013) Irradiation of an accretion disc by a jet: general properties and implications for spin measurements of black holes. *MNRAS*430:1694–1708. <https://doi.org/10.1093/mnras/sts710>, [arXiv:1301.4922](https://arxiv.org/abs/1301.4922) [astro-ph.HE]
- Dauser T, Garcia J, Parker ML, et al (2014)

- The role of the reflection fraction in constraining black hole spin. *MNRAS*444:L100–L104. <https://doi.org/10.1093/mnrasl/slu125>, [arXiv:1408.2347](https://arxiv.org/abs/1408.2347) [astro-ph.HE]
- Dauser T, García J, Walton DJ, et al (2016) Normalizing a relativistic model of X-ray reflection. Definition of the reflection fraction and its implementation in relxill. *A&A*590:A76. <https://doi.org/10.1051/0004-6361/201628135>, [arXiv:1601.03771](https://arxiv.org/abs/1601.03771) [astro-ph.HE]
- Degenaar N, Miller JM, Harrison FA, et al (2014) High-resolution X-Ray Spectroscopy of the Bursting Pulsar GRO J1744-28. *ApJL*796(1):L9. <https://doi.org/10.1088/2041-8205/796/1/L9>, [arXiv:1410.4841](https://arxiv.org/abs/1410.4841) [astro-ph.HE]
- Degenaar N, Miller JM, Chakrabarty D, et al (2015) A NuSTAR observation of disc reflection from close to the neutron star in 4U 1608-52. *MNRAS*451:L85–L89. <https://doi.org/10.1093/mnras/slv072>, [arXiv:1505.07112](https://arxiv.org/abs/1505.07112) [astro-ph.HE]
- Degenaar N, Altamirano D, Parker M, et al (2016) Disc reflection and a possible disc wind during a soft X-ray state in the neutron star low-mass X-ray binary 1RXS J180408.9-342058. *MNRAS*461(4):4049–4058. <https://doi.org/10.1093/mnras/stw1593>, [arXiv:1607.01780](https://arxiv.org/abs/1607.01780) [astro-ph.HE]
- Degenaar N, Ballantyne DR, Belloni T, et al (2018) Accretion Disks and Coronae in the X-Ray Flashlight. *Space Sci. Rev.*214(1):15. <https://doi.org/10.1007/s11214-017-0448-3>, [arXiv:1711.06272](https://arxiv.org/abs/1711.06272) [astro-ph.HE]
- Díaz Trigo M, Sidoli L, Boirin L, et al (2012) XMM-Newton observations of GX 13 + 1: correlation between photoionised absorption and broad line emission. *A&A*543:A50. <https://doi.org/10.1051/0004-6361/201219049>, [arXiv:1204.5904](https://arxiv.org/abs/1204.5904) [astro-ph.HE]
- Done C, Diaz Trigo M (2010) A re-analysis of the iron line in the XMM-Newton data from the low/hard state in GX339-4. *MNRAS*407(4):2287–2296. <https://doi.org/10.1111/j.1365-2966.2010.17092.x>, [arXiv:0911.3243](https://arxiv.org/abs/0911.3243) [astro-ph.HE]
- Done C, Gierliński M (2006) Truncated disc versus extremely broad iron line in XTE J1650-500. *MNRAS*367(2):659–668. <https://doi.org/10.1111/j.1365-2966.2005.09968.x>, [arXiv:astro-ph/0510614](https://arxiv.org/abs/astro-ph/0510614) [astro-ph]
- Done C, Gierliński M, Kubota A (2007) Modelling the behaviour of accretion flows in X-ray binaries. Everything you always wanted to know about accretion but were afraid to ask. *A&A Rev.*15(1):1–66. <https://doi.org/10.1007/s00159-007-0006-1>, [arXiv:0708.0148](https://arxiv.org/abs/0708.0148) [astro-ph]
- Esin AA, McClintock JE, Narayan R (1997) Advection-Dominated Accretion and the Spectral States of Black Hole X-Ray Binaries: Application to Nova Muscae 1991. *ApJ*489(2):865–889. <https://doi.org/10.1086/304829>, [arXiv:astro-ph/9705237](https://arxiv.org/abs/astro-ph/9705237) [astro-ph]
- Fabian AC, Rees MJ, Stella L, et al (1989) X-ray fluorescence from the inner disc in Cygnus X-1. *MNRAS*238:729–736
- Fabian AC, Iwasawa K, Reynolds CS, et al (2000) Broad Iron Lines in Active Galactic Nuclei. *PASP*112(775):1145–1161. <https://doi.org/10.1086/316610>, [arXiv:astro-ph/0004366](https://arxiv.org/abs/astro-ph/0004366) [astro-ph]
- Farinelli R, Fabiani S, Poutanen J, et al (2023) Accretion geometry of the neutron star low mass X-ray binary Cyg X-2 from X-ray polarization measurements. *MNRAS*519(3):3681–3690. <https://doi.org/10.1093/mnras/stac3726>, [arXiv:2212.13119](https://arxiv.org/abs/2212.13119) [astro-ph.HE]
- Fiocchi M, Bazzano A, Bruni G, et al (2019) Quasi-simultaneous INTEGRAL, SWIFT, and NuSTAR Observations of the New X-Ray Clocked Burster 1RXS J180408.9-342058. *ApJ*887(1):30. <https://doi.org/10.3847/1538-4357/ab4d59>, [arXiv:1910.09325](https://arxiv.org/abs/1910.09325) [astro-ph.HE]
- Frank J, King A, Raine DJ (2002) *Accretion Power in Astrophysics: Third Edition*
- Galloway DK, Munro MP, Hartman JM, et al (2008) Thermonuclear (Type I) X-Ray Bursts Observed by the Rossi X-Ray Timing Explorer. *ApJS*179(2):360–422. <https://doi.org/10.1086/>

- 592044, [arXiv:astro-ph/0608259](https://arxiv.org/abs/astro-ph/0608259) [astro-ph]
- García J, Kallman TR (2010) X-ray Reflected Spectra from Accretion Disk Models. I. Constant Density Atmospheres. *ApJ*718:695–706. <https://doi.org/10.1088/0004-637X/718/2/695>, [arXiv:1006.0485](https://arxiv.org/abs/1006.0485) [astro-ph.HE]
- García J, Kallman TR, Mushotzky RF (2011) X-ray Reflected Spectra from Accretion Disk Models. II. Diagnostic Tools for X-ray Observations. *ApJ*731(2):131. <https://doi.org/10.1088/0004-637X/731/2/131>, [arXiv:1101.1115](https://arxiv.org/abs/1101.1115) [astro-ph.HE]
- García J, Dauser T, Reynolds CS, et al (2013) X-Ray Reflected Spectra from Accretion Disk Models. III. A Complete Grid of Ionized Reflection Calculations. *ApJ*768(2):146. <https://doi.org/10.1088/0004-637X/768/2/146>, [arXiv:1303.2112](https://arxiv.org/abs/1303.2112) [astro-ph.HE]
- García J, Dauser T, Lohfink A, et al (2014a) Improved Reflection Models of Black Hole Accretion Disks: Treating the Angular Distribution of X-Rays. *ApJ*782(2):76. <https://doi.org/10.1088/0004-637X/782/2/76>, [arXiv:1312.3231](https://arxiv.org/abs/1312.3231) [astro-ph.HE]
- García JA, McClintock JE, Steiner JF, et al (2014b) An Empirical Method for Improving the Quality of RXTE PCA Spectra. *ApJ*794(1):73. <https://doi.org/10.1088/0004-637X/794/1/73>, [arXiv:1408.3607](https://arxiv.org/abs/1408.3607) [astro-ph.HE]
- García JA, Fabian AC, Kallman TR, et al (2016) The effects of high density on the X-ray spectrum reflected from accretion discs around black holes. *MNRAS*462(1):751–760. <https://doi.org/10.1093/mnras/stw1696>, [arXiv:1603.05259](https://arxiv.org/abs/1603.05259) [astro-ph.HE]
- García JA, Kallman TR, Bautista M, et al (2018) The Problem of the High Iron Abundance in Accretion Disks around Black Holes. In: Workshop on Astrophysical Opacities, p 282, <https://doi.org/10.48550/arXiv.1805.00581>, [1805.00581](https://arxiv.org/abs/1805.00581)
- García JA, Dauser T, Ludlam R, et al (2022) Relativistic X-Ray Reflection Models for Accreting Neutron Stars. *ApJ*926(1):13. <https://doi.org/10.3847/1538-4357/ac3cb7>, [arXiv:2111.12838](https://arxiv.org/abs/2111.12838) [astro-ph.HE]
- Garmire GP, Bautz MW, Ford PG, et al (2003) Advanced CCD imaging spectrometer (ACIS) instrument on the Chandra X-ray Observatory. In: Truemper JE, Tananbaum HD (eds) X-Ray and Gamma-Ray Telescopes and Instruments for Astronomy., pp 28–44, <https://doi.org/10.1117/12.461599>
- Gehrels N, Chincarini G, Giommi P, et al (2004) The Swift Gamma-Ray Burst Mission. *ApJ*611(2):1005–1020. <https://doi.org/10.1086/422091>, [arXiv:astro-ph/0405233](https://arxiv.org/abs/astro-ph/0405233) [astro-ph]
- Gendreau KC, Arzoumanian Z, Okajima T (2012) The Neutron star Interior Composition Explorer (NICER): an Explorer mission of opportunity for soft x-ray timing spectroscopy. In: Takahashi T, Murray SS, den Herder JWA (eds) Space Telescopes and Instrumentation 2012: Ultraviolet to Gamma Ray, Society of Photo-Optical Instrumentation Engineers (SPIE) Conference Series, vol 8443. SPIE, Bellingham, WA, p 844313, <https://doi.org/10.1117/12.926396>
- Harrison FA, Craig WW, Christensen FE, et al (2013) The Nuclear Spectroscopic Telescope Array (NuSTAR) High-energy X-Ray Mission. *ApJ*770(2):103. <https://doi.org/10.1088/0004-637X/770/2/103>, [arXiv:1301.7307](https://arxiv.org/abs/1301.7307) [astro-ph.IM]
- Hasinger G, van der Klis M (1989) Two patterns of correlated X-ray timing and spectral behaviour in low-mass X-ray binaries. *A&A*225:79–96
- Homan J, van der Klis M, Fridriksson JK, et al (2010) XTE J1701–462 and Its Implications for the Nature of Subclasses in Low-magnetic-field Neutron Star Low-mass X-ray Binaries. *ApJ*719(1):201–212. <https://doi.org/10.1088/0004-637X/719/1/201>, [arXiv:1005.3210](https://arxiv.org/abs/1005.3210) [astro-ph.HE]
- Ibragimov A, Poutanen J (2009) Accreting millisecond pulsar SAX J1808.4–3658 during its 2002 outburst: evidence for a receding disc. *MNRAS*400(1):492–508. <https://doi.org/10.1111/j.1365-2955.2009.13652.x>

- [//doi.org/10.1111/j.1365-2966.2009.15477.x](https://doi.org/10.1111/j.1365-2966.2009.15477.x),
arXiv:0901.0073 [astro-ph.SR]
- Inogamov NA, Sunyaev RA (1999) Spread of matter over a neutron-star surface during disk accretion. *Astronomy Letters* 25(5):269–293. <https://doi.org/10.48550/arXiv.astro-ph/9904333>, arXiv:astro-ph/9904333 [astro-ph]
- Jansen F, Lumb D, Altieri B, et al (2001) XMM-Newton observatory. I. The spacecraft and operations. *A&A*365:L1–L6. <https://doi.org/10.1051/0004-6361:20000036>
- Jayasurya KM, Agrawal VK, Chatterjee R (2023) Detection of significant X-ray polarization from transient NS-LMXB XTE J1701-462 with IXPE and its implication on the coronal geometry. *MNRAS*525(3):4657–4662. <https://doi.org/10.1093/mnras/stad2601>, arXiv:2302.03396 [astro-ph.HE]
- King AL, Tomsick JA, Miller JM, et al (2016) Measuring a Truncated Disk in Aquila X-1. *ApJL*819(2):L29. <https://doi.org/10.3847/2041-8205/819/2/L29>, arXiv:1602.07664 [astro-ph.HE]
- Kolehmainen M, Done C, Díaz Trigo M (2011) Modelling the high-mass accretion rate spectra of GX 339-4: black hole spin from reflection? *MNRAS*416(1):311–321. <https://doi.org/10.1111/j.1365-2966.2011.19040.x>, arXiv:1103.1256 [astro-ph.HE]
- Kubota A, Makishima K, Ebisawa K (2001) Observational Evidence for Strong Disk Comptonization in GRO J1655-40. *ApJL*560(2):L147–L150. <https://doi.org/10.1086/324377>, arXiv:astro-ph/0105426 [astro-ph]
- Kuulkers E, den Hartog PR, in't Zand JJM, et al (2003) Photospheric radius expansion X-ray bursts as standard candles. *A&A*399:663–680. <https://doi.org/10.1051/0004-6361:20021781>, arXiv:astro-ph/0212028 [astro-ph]
- Lamb FK, Boutloukos S, Van Wassenhove S, et al (2009) A Model for the Waveform Behavior of Accreting Millisecond X-Ray Pulsars: Nearly Aligned Magnetic Fields and Moving Emission Regions. *ApJ*706(1):417–435. <https://doi.org/10.1088/0004-637X/706/1/417>, arXiv:0808.4159 [astro-ph]
- Laor A (1991) Line Profiles from a Disk around a Rotating Black Hole. *ApJ*376:90. <https://doi.org/10.1086/170257>
- Lattimer JM (2011) Neutron stars and the dense matter equation of state. *Ap&SS*336(1):67–74. <https://doi.org/10.1007/s10509-010-0529-1>
- Lattimer JM, Prakash M (2001) Neutron Star Structure and the Equation of State. *ApJ*550(1):426–442. <https://doi.org/10.1086/319702>, arXiv:astro-ph/0002232 [astro-ph]
- Lattimer JM, Prakash M (2004) The Physics of Neutron Stars. *Science* 304(5670):536–542. <https://doi.org/10.1126/science.1090720>, arXiv:astro-ph/0405262 [astro-ph]
- Laurent P, Titarchuk L (2007) Effects of Downscattering on the Continuum and Line Spectra in a Powerful Wind Environment: Monte Carlo Simulations, Analytical Results, and Data Analysis. *ApJ*656(2):1056–1074. <https://doi.org/10.1086/510572>, arXiv:astro-ph/0611156 [astro-ph]
- Lin D, Remillard RA, Homan J (2007) Evaluating Spectral Models and the X-Ray States of Neutron Star X-Ray Transients. *ApJ*667(2):1073–1086. <https://doi.org/10.1086/521181>, arXiv:astro-ph/0702089 [astro-ph]
- Lin D, Remillard RA, Homan J (2010) Suzaku and BeppoSAX X-ray Spectra of the Persistently Accreting Neutron-star Binary 4U 1705–44. *ApJ*719(2):1350–1361. <https://doi.org/10.1088/0004-637X/719/2/1350>, arXiv:1006.5168 [astro-ph.HE]
- Liu H, Jiang J, Zhang Z, et al (2023) High-density Reflection Spectroscopy of Black Hole X-Ray Binaries in the Hard State. *ApJ*951(2):145. <https://doi.org/10.3847/1538-4357/acd8b9>, arXiv:2303.10593 [astro-ph.HE]
- Ludlam RM, Miller JM, Cackett EM, et al

- (2016) NuSTAR and XMM-Newton Observations of the Neutron Star X-Ray Binary 1RXS J180408.9-34205. *ApJ*824(1):37. <https://doi.org/10.3847/0004-637X/824/1/37>, [arXiv:1604.04252](https://arxiv.org/abs/1604.04252) [astro-ph.HE]
- Ludlam RM, Miller JM, Bachetti M, et al (2017a) A Hard Look at the Neutron Stars and Accretion Disks in 4U 1636-53, GX 17+2, and 4U 1705-44 with NuStar. *ApJ*836(1):140. <https://doi.org/10.3847/1538-4357/836/1/140>, [arXiv:1701.01774](https://arxiv.org/abs/1701.01774) [astro-ph.HE]
- Ludlam RM, Miller JM, Cackett EM, et al (2017b) Relativistic Disk Reflection in the Neutron Star X-Ray Binary XTE J1709-267 with NuSTAR. *ApJ*838(2):79. <https://doi.org/10.3847/1538-4357/aa661a>, [arXiv:1703.03103](https://arxiv.org/abs/1703.03103) [astro-ph.HE]
- Ludlam RM, Miller JM, Degenaar N, et al (2017c) Truncation of the Accretion Disk at One-third of the Eddington Limit in the Neutron Star Low-mass X-Ray Binary Aquila X-1. *ApJ*847(2):135. <https://doi.org/10.3847/1538-4357/aa8b1b>, [arXiv:1709.01559](https://arxiv.org/abs/1709.01559) [astro-ph.HE]
- Ludlam RM, Miller JM, Arzoumanian Z, et al (2018) Detection of Reflection Features in the Neutron Star Low-mass X-Ray Binary Serpens X-1 with NICER. *ApJL*858(1):L5. <https://doi.org/10.3847/2041-8213/aabee6>, [arXiv:1804.10214](https://arxiv.org/abs/1804.10214) [astro-ph.HE]
- Ludlam RM, Miller JM, Barret D, et al (2019a) NuSTAR Observations of the Accreting Atolls GX 3+1, 4U 1702-429, 4U 0614+091, and 4U 1746-371. *ApJ*873(1):99. <https://doi.org/10.3847/1538-4357/ab0414>, [arXiv:1902.00520](https://arxiv.org/abs/1902.00520) [astro-ph.HE]
- Ludlam RM, Shishkovsky L, Bult PM, et al (2019b) Observations of the Ultracompact X-Ray Binary 4U 1543-624 in Outburst with NICER, INTEGRAL, Swift, and ATCA. *ApJ*883(1):39. <https://doi.org/10.3847/1538-4357/ab3806>, [arXiv:1908.00539](https://arxiv.org/abs/1908.00539) [astro-ph.HE]
- Ludlam RM, Cackett EM, García JA, et al (2020) NICER-NuSTAR Observations of the Neutron Star Low-mass X-Ray Binary 4U 1735-44. *ApJ*895(1):45. <https://doi.org/10.3847/1538-4357/ab89a6>, [arXiv:2004.06723](https://arxiv.org/abs/2004.06723) [astro-ph.HE]
- Ludlam RM, Jaodand AD, García JA, et al (2021) Simultaneous NICER and NuSTAR Observations of the Ultracompact X-Ray Binary 4U 1543-624. *ApJ*911(2):123. <https://doi.org/10.3847/1538-4357/abedb0>, [arXiv:2012.10461](https://arxiv.org/abs/2012.10461) [astro-ph.HE]
- Ludlam RM, Cackett EM, García JA, et al (2022) Radius Constraints from Reflection Modeling of Cygnus X-2 with NuSTAR and NICER. *ApJ*927(1):112. <https://doi.org/10.3847/1538-4357/ac5028>, [arXiv:2201.11767](https://arxiv.org/abs/2201.11767) [astro-ph.HE]
- Ludlam RM, Malacaria C, Sokolova-Lapa E, et al (2023) The High Energy X-ray Probe (HEX-P): A New Window into Neutron Star Accretion. *arXiv e-prints* [arXiv:2311.04687](https://arxiv.org/abs/2311.04687). <https://doi.org/10.48550/arXiv.2311.04687>, [arXiv:2311.04687](https://arxiv.org/abs/2311.04687) [astro-ph.HE]
- Madej OK, Jonker PG (2011) Discovery of a broad O VIII Ly α line in the ultracompact X-ray binary 4U 1543-624. *MNRAS*412(1):L11–L15. <https://doi.org/10.1111/j.1745-3933.2010.00989.x>, [arXiv:1011.2763](https://arxiv.org/abs/1011.2763) [astro-ph.HE]
- Madej OK, García J, Jonker PG, et al (2014) X-ray reflection in oxygen-rich accretion discs of ultracompact X-ray binaries. *MNRAS*442(2):1157–1165. <https://doi.org/10.1093/mnras/stu884>, [arXiv:1403.1432](https://arxiv.org/abs/1403.1432) [astro-ph.HE]
- Magdziarz P, Zdziarski AA (1995) Angle-dependent Compton reflection of X-rays and gamma-rays. *MNRAS*273(3):837–848. <https://doi.org/10.1093/mnras/273.3.837>
- Marino A, Russell TD, Del Santo M, et al (2023) The accretion/ejection link in the neutron star X-ray binary 4U 1820-30 I: a boundary layer-jet coupling? *MNRAS*525(2):2366–2379. <https://doi.org/10.1093/mnras/stad2386>, [arXiv:2307.16566](https://arxiv.org/abs/2307.16566) [astro-ph.HE]

- Matranga M, Di Salvo T, Iaria R, et al (2017) A re-analysis of the NuSTAR and XMM-Newton broad-band spectrum of Serpens X-1. *A&A*600:A24. <https://doi.org/10.1051/0004-6361/201628576>, [arXiv:1701.01069](https://arxiv.org/abs/1701.01069) [astro-ph.HE]
- Meidinger N (2018) The Wide Field Imager instrument for Athena. *Contributions of the Astronomical Observatory Skalnaté Pleso* 48(3):498–505. <https://doi.org/10.48550/arXiv.1702.01079>, [arXiv:1702.01079](https://arxiv.org/abs/1702.01079) [astro-ph.IM]
- Miller JM, Fabian AC, Reynolds CS, et al (2002) Revealing Evidence of Spin in Galactic Black Holes. In: *American Astronomical Society Meeting Abstracts*, p 57.01
- Miller JM, Reynolds CS, Fabian AC, et al (2009) Stellar-Mass Black Hole Spin Constraints from Disk Reflection and Continuum Modeling. *ApJ*697(1):900–912. <https://doi.org/10.1088/0004-637X/697/1/900>, [arXiv:0902.2840](https://arxiv.org/abs/0902.2840) [astro-ph.HE]
- Miller JM, D’Aì A, Bautz MW, et al (2010) On Relativistic Disk Spectroscopy in Compact Objects with X-ray CCD Cameras. *ApJ*724(2):1441–1455. <https://doi.org/10.1088/0004-637X/724/2/1441>, [arXiv:1009.4391](https://arxiv.org/abs/1009.4391) [astro-ph.HE]
- Miller JM, Maitra D, Cackett EM, et al (2011) A Fast X-ray Disk Wind in the Transient Pulsar IGR J17480–2446 in Terzan 5. *ApJL*731(1):L7. <https://doi.org/10.1088/2041-8205/731/1/L7>, [arXiv:1101.2377](https://arxiv.org/abs/1101.2377) [astro-ph.HE]
- Miller JM, Raymond J, Fabian AC, et al (2012) The Disk-wind-Jet Connection in the Black Hole H 1743-322. *ApJL*759(1):L6. <https://doi.org/10.1088/2041-8205/759/1/L6>, [arXiv:1208.4514](https://arxiv.org/abs/1208.4514) [astro-ph.HE]
- Miller JM, Parker ML, Fuerst F, et al (2013) Constraints on the Neutron Star and Inner Accretion Flow in Serpens X-1 Using NuSTAR. *ApJL*779(1):L2. <https://doi.org/10.1088/2041-8205/779/1/L2>, [arXiv:1310.5776](https://arxiv.org/abs/1310.5776) [astro-ph.HE]
- Mitsuda K, Inoue H, Nakamura N, et al (1989) Luminosity-related changes of the energy spectrum of X 1608–522. *PASJ*41:97–111
- Mitsuda K, Bautz M, Inoue H, et al (2007) The X-Ray Observatory Suzaku. *PASJ*59:S1–S7. <https://doi.org/10.1093/pasj/59.sp1.S1>
- Mondal AS, Dewangan GC, Pahari M, et al (2018) NuSTAR view of the Z-type neutron star low-mass X-ray binary Cygnus X-2. *MNRAS*474(2):2064–2072. <https://doi.org/10.1093/mnras/stx2931>, [arXiv:1708.01032](https://arxiv.org/abs/1708.01032) [astro-ph.HE]
- Mondal AS, Dewangan GC, Raychaudhuri B (2020) On the disc reflection spectroscopy of NS LMXB Serpens X-1: analysis of a recent NuSTAR observation. *MNRAS*494(3):3177–3185. <https://doi.org/10.1093/mnras/staa1001>, [arXiv:1907.08625](https://arxiv.org/abs/1907.08625) [astro-ph.HE]
- Moutard DL, Ludlam RM, García JA, et al (2023) Simultaneous NICER and NuSTAR Observations of the Ultracompact X-Ray Binary 4U 0614+091. *ApJ*957(1):27. <https://doi.org/10.3847/1538-4357/acf4f3>, [arXiv:2308.15581](https://arxiv.org/abs/2308.15581) [astro-ph.HE]
- Mukherjee D, Bult P, van der Klis M, et al (2015) The magnetic-field strengths of accreting millisecond pulsars. *MNRAS*452(4):3994–4012. <https://doi.org/10.1093/mnras/stv1542>, [arXiv:1507.02138](https://arxiv.org/abs/1507.02138) [astro-ph.HE]
- Nandra K, Barret D, Barcons X, et al (2013) The Hot and Energetic Universe: A White Paper presenting the science theme motivating the Athena+ mission. *arXiv e-prints* [arXiv:1306.2307](https://arxiv.org/abs/1306.2307). <https://doi.org/10.48550/arXiv.1306.2307>, [arXiv:1306.2307](https://arxiv.org/abs/1306.2307) [astro-ph.HE]
- Narayan R, Yi I (1994) Advection-dominated Accretion: A Self-similar Solution. *ApJL*428:L13. <https://doi.org/10.1086/187381>, [arXiv:astro-ph/9403052](https://arxiv.org/abs/astro-ph/9403052) [astro-ph]
- Nelemans G, Jonker PG, Marsh TR, et al (2004) Optical spectra of the carbon-oxygen accretion discs in the ultra-compact X-ray binaries 4U 0614+09, 4U 1543-624 and 2S 0918-549. *MNRAS*348(1):L7–L11. <https://doi.org/>

- 10.1111/j.1365-2966.2004.07486.x, [arXiv:astro-ph/0312008](#) [astro-ph]
- Ng C, Díaz Trigo M, Cadolle Bel M, et al (2010) A systematic analysis of the broad iron $K\alpha$ line in neutron-star LMXBs with XMM-Newton. *A&A*522:A96. <https://doi.org/10.1051/0004-6361/200913575>, [arXiv:1005.3755](#) [astro-ph.HE]
- Ng M, Hughes AK, Homan J, et al (2023) X-ray and Radio Monitoring of the Neutron Star Low Mass X-ray Binary 1A 1744-361: Quasi Periodic Oscillations, Transient Ejections, and a Disk Atmosphere. *arXiv e-prints arXiv:2310.01511*. <https://doi.org/10.48550/arXiv.2310.01511>, [arXiv:2310.01511](#) [astro-ph.HE]
- Özel F, Freire P (2016) Masses, Radii, and the Equation of State of Neutron Stars. *ARA&A*54:401–440. <https://doi.org/10.1146/annurev-astro-081915-023322>, [arXiv:1603.02698](#) [astro-ph.HE]
- Papitto A, Di Salvo T, D’Ai A, et al (2009) XMM-Newton detects a relativistically broadened iron line in the spectrum of the ms X-ray pulsar SAX J1808.4-3658. *A&A*493(3):L39–L43. <https://doi.org/10.1051/0004-6361:200811401>, [arXiv:0812.1149](#) [astro-ph]
- Parikh AS, Wijnands R, Degenaar N, et al (2017) Very hard states in neutron star low-mass X-ray binaries. *MNRAS*468(4):3979–3984. <https://doi.org/10.1093/mnras/stx747>, [arXiv:1703.09497](#) [astro-ph.HE]
- Popham R, Sunyaev R (2001) Accretion Disk Boundary Layers around Neutron Stars: X-Ray Production in Low-Mass X-Ray Binaries. *ApJ*547(1):355–383. <https://doi.org/10.1086/318336>, [arXiv:astro-ph/0004017](#) [astro-ph]
- Reynolds CS (2014) Measuring Black Hole Spin Using X-Ray Reflection Spectroscopy. *Space Sci. Rev.*183(1-4):277–294. <https://doi.org/10.1007/s11214-013-0006-6>, [arXiv:1302.3260](#) [astro-ph.HE]
- Reynolds CS (2021) Observational Constraints on Black Hole Spin. *ARA&A*59:117–154. <https://doi.org/10.1146/annurev-astro-112420-035022>, [arXiv:2011.08948](#) [astro-ph.HE]
- Ross RR, Fabian AC (2005) A comprehensive range of X-ray ionized-reflection models. *MNRAS*358:211–216. <https://doi.org/10.1111/j.1365-2966.2005.08797.x>, [arXiv:astro-ph/0501116](#)
- Ross RR, Fabian AC, Young AJ (1999) X-ray reflection spectra from ionized slabs. *MNRAS*306(2):461–466. <https://doi.org/10.1046/j.1365-8711.1999.02528.x>, [arXiv:astro-ph/9902325](#) [astro-ph]
- Saavedra EA, García F, Fogantini FA, et al (2023) Relativistic X-ray reflection and photoionized absorption in the neutron star low-mass X-ray binary GX 13+1. *MNRAS*522(3):3367–3377. <https://doi.org/10.1093/mnras/stad1157>, [arXiv:2304.03130](#) [astro-ph.HE]
- Shakura NI, Sunyaev RA (1973) Black holes in binary systems. Observational appearance. *A&A*24:337–355
- Shimura T, Takahara F (1995) On the Spectral Hardening Factor of the X-Ray Emission from Accretion Disks in Black Hole Candidates. *ApJ*445:780. <https://doi.org/10.1086/175740>
- Sibgatullin NR, Sunyaev RA (1998) Disk accretion in the gravitational field of a rapidly rotating neutron star with a rotationally induced quadrupole mass distribution. *Astronomy Letters* 24(6):774–787. <https://doi.org/10.48550/arXiv.astro-ph/9811028>, [arXiv:astro-ph/9811028](#) [astro-ph]
- Sleator CC, Tomsick JA, King AL, et al (2016) A NuSTAR Observation of the Reflection Spectrum of the Low-mass X-Ray Binary 4U 1728-34. *ApJ*827(2):134. <https://doi.org/10.3847/0004-637X/827/2/134>, [arXiv:1605.02137](#) [astro-ph.HE]
- Sunyaev RA, Arefev VA, Borozdin KN, et al (1991) Broadband X-Ray Spectra of Black-Hole Candidates X-Ray Pulsars and Low-Mass Binary X-Ray Systems - KVANT Module Results. *Soviet Astronomy Letters* 17:409

- Tanaka Y, Nandra K, Fabian AC, et al (1995) Gravitationally redshifted emission implying an accretion disk and massive black hole in the active galaxy MCG-6-30-15. *Nature*375(6533):659–661. <https://doi.org/10.1038/375659a0>
- Tarter CB, Tucker WH, Salpeter EE (1969) The Interaction of X-Ray Sources with Optically Thin Environments. *ApJ*156:943. <https://doi.org/10.1086/150026>
- Tashiro M, Maejima H, Toda K, et al (2018) Concept of the X-ray Astronomy Recovery Mission. In: den Herder JWA, Nikzad S, Nakazawa K (eds) *Space Telescopes and Instrumentation 2018: Ultraviolet to Gamma Ray*, p 1069922, <https://doi.org/10.1117/12.2309455>
- Titarchuk L, Laurent P, Shaposhnikov N (2009) On the Nonrelativistic Origin of Red-skewed Iron Lines in Cataclysmic Variable, Neutron Star, and Black Hole Sources. *ApJ*700(2):1831–1846. <https://doi.org/10.1088/0004-637X/700/2/1831>, [arXiv:0906.1490](https://arxiv.org/abs/0906.1490) [astro-ph.HE]
- Tomsick JA, Parker ML, García JA, et al (2018) Alternative Explanations for Extreme Supersolar Iron Abundances Inferred from the Energy Spectrum of Cygnus X-1. *ApJ*855(1):3. <https://doi.org/10.3847/1538-4357/aaaab1>, [arXiv:1801.07267](https://arxiv.org/abs/1801.07267) [astro-ph.HE]
- Ursini F, Farinelli R, Gnarini A, et al (2023) X-ray polarimetry and spectroscopy of the neutron star low-mass X-ray binary GX 9+9: An in-depth study with IXPE and NuSTAR. *A&A*676:A20. <https://doi.org/10.1051/0004-6361/202346541>, [arXiv:2306.02740](https://arxiv.org/abs/2306.02740) [astro-ph.HE]
- van den Eijnden J, Bagnoli T, Degenaar N, et al (2017) A strongly truncated inner accretion disc in the Rapid Burster. *MNRAS*466(1):L98–L102. <https://doi.org/10.1093/mnrasl/slw244>, [arXiv:1612.00384](https://arxiv.org/abs/1612.00384) [astro-ph.HE]
- van den Eijnden J, Degenaar N, Pinto C, et al (2018) The very faint X-ray binary IGR J17062-6143: a truncated disc, no pulsations, and a possible outflow. *MNRAS*475(2):2027–2044. <https://doi.org/10.1093/mnras/stx3224>
- van den Eijnden J, Degenaar N, Ludlam RM, et al (2020) A strongly changing accretion morphology during the outburst decay of the neutron star X-ray binary 4U 1608-52. *MNRAS*493(1):1318–1327. <https://doi.org/10.1093/mnras/staa423>, [arXiv:2002.04003](https://arxiv.org/abs/2002.04003) [astro-ph.HE]
- van der Klis M (2005) Timing Neutron Stars. In: *The Electromagnetic Spectrum of Neutron Stars*, p 283
- Wang Y, Méndez M, Sanna A, et al (2017) The reflection spectrum of the low-mass X-ray binary 4U 1636-53. *MNRAS*468(2):2256–2264. <https://doi.org/10.1093/mnras/stx671>, [arXiv:1703.05607](https://arxiv.org/abs/1703.05607) [astro-ph.HE]
- Weisskopf MC, Soffitta P, Baldini L, et al (2022) The Imaging X-Ray Polarimetry Explorer (IXPE): Pre-Launch. *Journal of Astronomical Telescopes, Instruments, and Systems* 8(2):026002. <https://doi.org/10.1117/1.JATIS.8.2.026002>, [arXiv:2112.01269](https://arxiv.org/abs/2112.01269) [astro-ph.IM]
- White NE, Stella L, Parmar AN (1988) The X-Ray Spectral Properties of Accretion Disks in X-Ray Binaries. *ApJ*324:363. <https://doi.org/10.1086/165901>
- Wilkins DR (2018) On the illumination of neutron star accretion discs. *MNRAS*475(1):748–756. <https://doi.org/10.1093/mnras/stx3167>, [arXiv:1712.02364](https://arxiv.org/abs/1712.02364) [astro-ph.HE]
- Wilkins DR, Fabian AC (2012) Understanding X-ray reflection emissivity profiles in AGN: locating the X-ray source. *MNRAS*424(2):1284–1296. <https://doi.org/10.1111/j.1365-2966.2012.21308.x>, [arXiv:1205.3179](https://arxiv.org/abs/1205.3179) [astro-ph.HE]
- Yamada S, Makishima K, Uehara Y, et al (2009) Is the Black Hole in GX 339-4 Really Spinning Rapidly? *ApJL*707(2):L109–L113. <https://doi.org/10.1088/0004-637X/707/2/L109>, [arXiv:0911.2306](https://arxiv.org/abs/0911.2306) [astro-ph.HE]
- Zimmerman ER, Narayan R, McClintock JE, et al (2005) Multitemperature Blackbody Spectra of Thin Accretion Disks with and without a Zero-Torque Inner Boundary Condition. *ApJ*618(2):832–844. <https://doi.org/10.1086/426888>

[1086/426071](#), [arXiv:astro-ph/0408209](#) [astro-ph]